ISSN: 2639-0108

Research Article

Advances in Theoretical & Computational Physics

Microwave Absorption Behavior of Low Loading Ratio of $Ni^{3+}_{0.25}Ni^{2+}_{0.375}Zn^{2+}_{0.25}Fe_2O_4$ Nanoparticles Coated with Polyaniline Within Paraffin Wax Matrix

Anas Houbi[1,2]*, Zharmenov Abdurassul Aldashevich[1,2], Yomen Atassi[3], Bagasharova Zhenisgul Telmanovna[1,2], Mirzalieva Saule[1,2]

[1]*National Center on Complex Processing of Mineral Raw Materials of the Republic of Kazakhstan, Almaty, Kazakhstan*

[2]*Department of Chemical Technology of Inorganic Substances, Al-Farabi Kazakh National University, Almaty, Kazakhstan*

[3]*Department of Applied Physics, Higher Institute for Applied Sciences and Technology, Damascus, Syria*

***Corresponding author**
Anas Houbi, National Center on Complex Processing of Mineral Raw Materials of the Republic of Kazakhstan, Almaty, Kazakhstan

Submitted: 09 May 2022; **Accepted:** 19 May 2022; **Published:** 28 May 2022

Citation: *Anas Houbi, Yomen Atassi, Zharmenov Abdurassul Aldashevich, Bagasharova Zhenisgul Telmanovna, Mirzalieva Saule. (2022). Microwave Absorption Behavior of Low Loading Ratio of $Ni^{3+}_{0.25}Ni^{2+}_{0.375}Zn^{2+}_{0.25}Fe_2O_4$ Nanoparticles Coated with Polyaniline Within Paraffin Wax Matrix. Adv Theo Comp Phy, 5(2), 436-448.*

Abstract

NiZn ferrite ($Ni^{3+}_{0.25}Ni^{2+}_{0.375}Zn^{2+}_{0.25}Fe_2O_4$) is coated with polyaniline (PANI) using an in-situ polymerization technique. Three various weight ratios of PANI/$Ni^{3+}_{0.25}Ni^{2+}_{0.375}Zn^{2+}_{0.25}Fe_2O_4$ (1:1, 2:1, and 3:1) are synthesized. The absorbers are synthesized by introducing PANI/F nanocomposites within a paraffin wax of 25% w/w. X-ray diffractometry, FTIR spectroscopy, UV-vis spectroscopy, TGA analysis and SEM analysis are utilized in order to characterize the samples. The electromagnetic interference (EMI) shielding and microwave absorption (MA) properties are measured in the frequency band of 8.8–12 GHz to investigate the microwave characterization. Minimal reflection loss of -19.8 dB at the matching frequency of 10.8 GHz and the absorption bandwidth under -10 dB of 2.2 GHz for 3.12 mm thickness with a surface density of 3.07 kg/m^2 are noticed for the PANI/F.2 nanocomposite sample. The maximum shielding efficiency of 23.18 dB at 11.1 GHz for 2.90 mm thickness is observed for the PANI/F.2 nanocomposite.

Keywords: NiZn Ferrite, PANI, Lightweight Microwave Absorber, Reflection Loss, Shielding Efficiency

Introduction

EMI would be regarded as an unwanted result of modern technology that has effects dangerous on human health, intelligent devices, telecommunication devices, and military industries. Consequently, the disposal of electromagnetic waves resulting from EMI effectively is so important both for public protection security and electronic safety [1–6]. Hence, it is significant to create solutions to protect human health and shield electronic devices from microwaves. Ferrites have distinguished unique magnetic properties which allow them to absorb microwaves because of the potential of spin changing. Ferrites have been classified according to the crystal structure to the spinel, hexagonal, garnet ferrites. Spinel and hexagonal ferrites have been well-known for their integral microwave absorption characteristics [7,8]. However, these ferrites are restrained because of high density, lower dielectric loss, and limited absorption band which makes use of these ferrites inefficient particularly when wideband absorption is required [9,10]. To find solutions for these shortcomings, dielectric loss materials are added, such as polyaniline, polypyrrole, carbon nanotubes, carbon black, etc. Where the results have shown the synergistic impact of combining magnetic loss and dielectric loss material together [11]. Polyaniline is one of the conductive polymers which has a conductivity in the band of semiconductors and it is characterized by its dielectric loss properties and low density. Many researchers have executed studies of the microwave absorption properties of spinel ferrite nanoparticles containing conductive polymers. According to this, PANI/NiZn ferrite microwave absorbers in the frequency range of 2–40 GHz were successfully prepared by Jau et al. [12]. The absorbers are synthesized by introducing PANI/NiZn ferrite nanocomposites within an epoxy resin matrix of 67% w/w. The results indicated that by increasing polyaniline content in NiZn ferrite, a wide absorption frequency range could be obtained. Ali et al. have designed microwave absorbers in the frequency band of 8-12 GHz based on PANI/MnNiZn ferrite at the weight ratio of 1:1. The absorbers are formed by dispersing PANI/MnNiZn ferrite within a paraffin matrix of 20–25% w/w. The results have shown that the absorber with a loading percentage within a paraffin matrix of 25% w/w had minimal reflection loss (RL_{min}) of -31.32 dB at 11.13 GHz and the absorption bandwidth under -10 dB (BW_{-10dB}) was 3.74 GHz for 3 mm thickness [13]. Xie et al. have reported

the MA characteristics of a one-dimensional uniform PANI/NiZn ferrite hybrid nanorods within a paraffin matrix of 70% w/w in the frequency range of 2-18 GHz. They have found that the absorbers had broadband, and minimal reflection loss, where the results have indicated that the absorber had a RL_{min} of -27.5 dB at 6.2 GHz and the absorption BW_{-10dB} was 3 GHz for 2 mm thickness [14]. Zhang et al. have prepared PANI/NiZn ferrite composites by in-situ polymerization within a paraffin matrix of 75% w/w. The molar ratios of PANI/NiZn ferrite were 3:1, 2:1, 1:1, 1:2, 1:3, where the optimal sample has exhibited PANI/NiZn at the molar ratio of 1:2 had a RLmin of -41 dB at 12.8 GHz and the absorption BW_{-10dB} was 5 GHz for 2.6 mm thickness [15]. In the present research, the impact of substituting $Ni_{0.5}Zn_{0.5}Fe_2O_4$ (NiZn ferrite) by nickel ion is studied on the MA and EMI shielding properties of PANI/F nanocomposite. Until now, to the best of our knowledge, no studies have been reported on the EMI shielding and MA properties of composites made up of PANI/F nanocomposite. The purpose of the study is to prepare MAMs that have high shielding effectiveness and minimal reflection loss with a weight ratio within a paraffin wax matrix of 25% w/w. The experimental process consists of preparing the spinel ferrite through a ceramic sintering technique. After that, the spinel ferrite is coated with PANI using an in-situ polymerization technique. Three various weight ratios of PANI/$Ni^{3+}_{0.25}Ni^{2+}_{0.375}Zn^{2+}_{0.25}Fe_2O_4$ (1:1, 2:1, and 3:1) are synthesized. The preparation of such nanocomposites is verified by different characterization methods involving X-ray diffractometry, FTIR spectroscopy, UV–vis spectroscopy, TGA analysis and SEM analysis. The EMI shielding and MA properties are studied by measuring the RL_{min}, BW_{-10dB}, and SE of the absorbers in the frequency band of 8.8–12 GHz to achieve functional characterization.

Experimental procedure

Synthesis of ferrite ($Ni^{3+}_{0.25}Ni^{2+}_{0.375}Zn^{2+}_{0.25}Fe_2O_4$) nanoparticles

NiZn ferrite ($Ni^{3+}_{0.25}Ni^{2+}_{0.375}Zn^{2+}_{0.25}Fe_2O_4$) nanoparticles were prepared by a ceramic sintering technique. $Ni^{3+}_{0.25}Ni^{2+}_{0.375}Zn^{2+}_{0.25}Fe_2O_4$ nanoparticles were synthesized by taking appropriate amounts of Iron(III) oxide (Fe_2O_3), Zinc(II) oxide (ZnO), Nickel(II) oxide (NiO) and Nickel(III) oxide (Ni2O3) were blended together and with ethanol solution with weight ratio (2:1) using the grinding balls for 8 h at 200 rpm, then the whole mixture was transferred to the furnace for disposal of the ethanol for 24 h at 70 °C. After that, the mixture was sintered for 3 h at 1100 °C. Finally, the prepared ferrite was milled again in the presence of ethanol solution for 4 h at 200 rpm and the whole mixture was transferred to the furnace for disposal of the ethanol for 24 h at 70 °C. The flow chart for the synthesis of ferrite utilizing the ceramic sintering technique is shown in Figure 1.

Coating NiZn ferrite nanoparticles with polyaniline

NiZn ferrite nanoparticles were coated with polyaniline via the in-situ polymerization technique. Firstly, 6 g of $Ni^{3+}_{0.25}Ni^{2+}_{0.375}Zn^{2+}_{0.25}Fe_2O_4$ was added to 100 ml distilled water under mechanical stirring at a speed of 250 rpm for 30 minutes. 3 g sodium dodecyl sulfate (SDS) and aniline were added to the solution while keeping mechanical stirring for 1 h. After that, 1 M HCl solution 80 mL was added to the solution under stirring for 1 h. Finally, 8.5 g APS was dissolved in 100 ml of an aqueous solution which was utilized as an oxidizing agent and added slowly dropwise into the solution to start the polymerization. The polymerization was allowed to proceed for 6 h with stirring in an ice bath. The resulting nanocomposite was filtered and washed many times with distilled water and ethanol, and then dried for 8 h in the furnace at 70 °C. The schematic diagram of a PANI/F by the in-situ polymerization technique is shown in Fig. 2. The nanocomposite ratios of $Ni^{3+}_{0.25}Ni^{2+}_{0.375}Zn^{2+}_{0.25}Fe_2O_4$ and aniline in weight were 1:1 (PANI/F.1), 2:1 (PANI/F.2) and 3:1 (PANI/F.3), respectively. Pure polyaniline was synthesized in a similar way but without NiZn ferrite solution for comparison purposes.

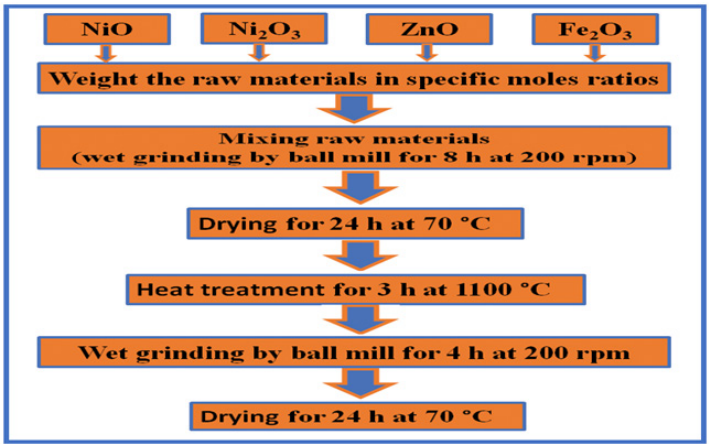

Figure 1: Flow chart for the synthesis of ferrite utilizing ceramic sintering technique.

Preparation of samples for measuring the MA and EMI shielding properties

Microwave absorption and electromagnetic interference shielding properties of the samples were estimated with the free-space technique. According to this, 25% w/w of the coated nanocomposite was dispersed in a paraffin wax matrix by heating and stirring for 15 min. Thereafter, the single-layer samples were molded to the dimensions of 100×100 mm to measure RL and SE in the frequency band of 8.8–12 GHz.

Measurements

A powder X-ray diffractometer (XRD, Rigaku Miniflex 600, Cu-Ka) is utilized for defining the crystal structures of the powders. Fourier Transform IR (FTIR) spectra are recorded on a Perkin Elmer spectrum 65 FTIR spectrometer in the range of 400–4000 cm-1. The UV–vis absorption spectra of the samples (dispersed in dimethylformamide (DMF)) was recorded using the LAMBDA 365 UV–vis spectrophotometer in the range of 250–900 nm. Thermogravimetric analysis (TGA) is done utilizing a thermal analyzer (NETZSCH 449F3A-0372-M) under a nitrogen atmosphere, from room temperature to 1000°C under constant heating rate of 10 °C/min. A scanning electron microscope (FEI Quanta 200 3D) is utilized for defining the morphology of the powders. Finally, energy-dispersive X-ray spectroscopy (EDX, Quanta 200 3D) is utilized to know the chemical composition of prepared samples. The EMI shielding and MA properties of the prepared samples are measured by using the horn antenna connected to an oscilloscope.

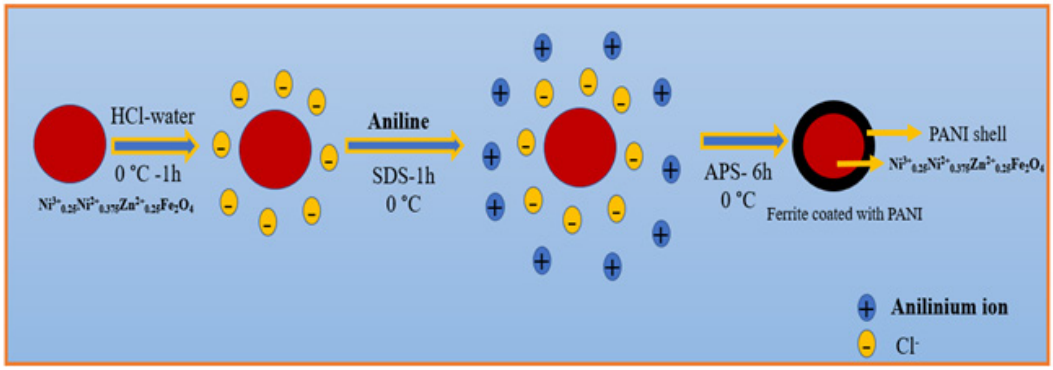

Figure 2: Schematic diagram of a polyaniline/NiZn ferrite by the in-situ polymerization technique.

Results and discussion

XRD patterns

Fig. 3 shows the XRD patterns of the $Ni^{3+}_{0.25}Ni^{2+}_{0.375}Zn^{2+}_{0.25}Fe_2O_4$, PANI/F nanocomposites and PANI. For the $Ni^{3+}_{0.25}Ni^{2+}_{0.375}Zn^{2+}_{0.25}Fe_2O_4$ pattern, eight diffraction peaks are noticed at 2θ values of 18.42°, 30.34°, 35.66°, 36.5°, 43.34°, 53.84°, 57.32°, and 63.02°, which conforms to (hkl) planes of (111), (220), (311), (222), (400), (422), (511) and (440), respectively. The ideal spinel structure is noticed by the peaks of NiZn ferrite [16]. All the observed peaks of the NiZn ferrite are matched with the standard XRD pattern (JCPDS, PDF no. 08–0234). The size of the NiZn ferrite grain (2θ =35.66°) has been evaluated with Scherrer's equation, D=0.9 λ/β cosθ, where D is the crystallite size (nm), λ is the X-ray wavelength, β is the bandwidth at half-height, and θ is the diffraction angle in degree. The calculated crystallite size of the NiZn ferrite is 20.7 nm. The characteristic peaks of PANI/F nanocomposites show matching the characteristic peaks of $Ni^{3+}_{0.25}Ni^{2+}_{0.375}Zn^{2+}_{0.25}Fe_2O_4$ core as mentioned above. This reveals when the $Ni^{3+}_{0.25}Ni^{2+}_{0.375}Zn^{2+}_{0.25}Fe_2O_4$ magnetic core is coated with PANI, the spinel structure of the $Ni^{3+}_{0.25}Ni^{2+}_{0.375}Zn^{2+}_{0.25}Fe_2O_4$ magnetic core remains intact. As shown in Fig. 3, the XRD pattern of the pure PANI displays an amorphous structure with two characteristic peaks at 20.22° and 25.36° which are attributed to the periodicity parallel to the polymer chains of PANI [17,18]. The XRD patterns of the PANI/ $Ni^{3+}_{0.25}Ni^{2+}_{0.375}Zn^{2+}_{0.25}Fe_2O_4$ nanocomposites (Fig. 3) display crystalline peaks because of the existence of NiZn ferrite in these nanocomposites. The two characteristic peaks of the PANI disappeared due to the $Ni^{3+}_{0.25}Ni^{2+}_{0.375}Zn^{2+}_{0.25}Fe_2O_4$ nanoparticles [19,20].

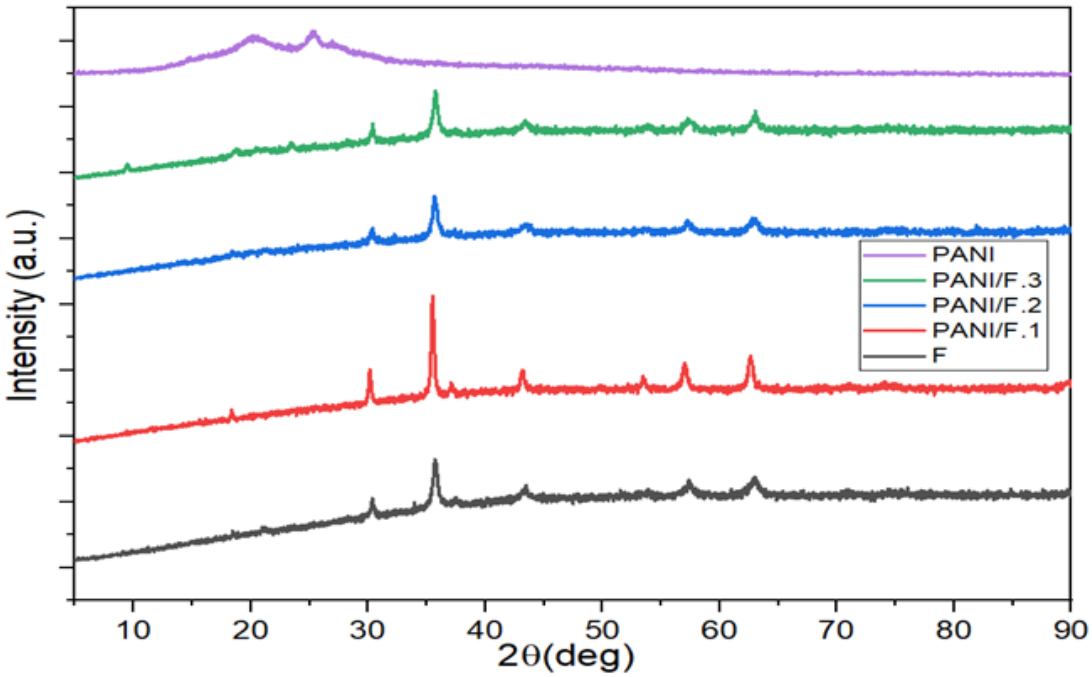

Figure 3: XRD patterns of $Ni^{3+}_{0.25}Ni^{2+}_{0.375}Zn^{2+}_{0.25}Fe_2O_4$, PANI/$Ni^{3+}_{0.25}Ni^{2+}_{0.375}Zn^{2+}_{0.25}Fe_2O_4$ nanocomposites and pure PANI.

FTIR spectra

The FTIR spectra of the $Ni^{3+}_{0.25}Ni^{2+}_{0.375}Zn^{2+}_{0.25}Fe_2O_4$, PANI/F nanocomposites and polyaniline are shown in Fig. 4. For the $Ni^{3+}_{0.25}Ni^{2+}_{0.375}Zn^{2+}_{0.25}Fe_2O_4$ nanoparticles, two peaks at 579.8 cm-1 and 445.3 cm-1 are referring to the stretching vibration of (Fe-O), which emphasizes the formation of the metal-oxygen in ferrite-based [21]. On the other hand, the characteristic peaks of PANI and PANI/F nanocomposites are similar and they exhibited peaks at 1568 cm^{-1}, 1489 cm^{-1}, 1298 cm^{-1}, 1238 cm^{-1}, 1113 cm^{-1}, and 800 cm^{-1} [22,23]. The characteristic peaks at 1568 and 1489 cm^{-1} are attributed to the C=N and C=C stretching modes of vibration for the quinonoid and benzenoid units of the polymer. The characteristic peaks at 1298 and 1238 cm-1 are related to N-H bending and asymmetric C-H stretching of the benzenoid ring, respectively. Finally, the characteristic peaks at 1113 cm-1 and 800 cm-1 are ascribed to the vibration mode of N=Q=N and the out-of-plane stretching vibration of C–H, respectively [15,19]. In addition to that, the characteristic peak at 579.8 cm^{-1} of PANI/F nanocomposites shows matching the characteristic peak of $Ni^{3+}_{0.25}Ni^{2+}_{0.375}Zn^{2+}_{0.25}Fe_2O_4$ core as mentioned above. This indicates the stretching vibration of (Fe-O), which confirms the formation of the metal-oxygen in PANI/$Ni^{3+}_{0.25}Ni^{2+}_{0.375}Zn^{2+}_{0.25}Fe_2O_4$.

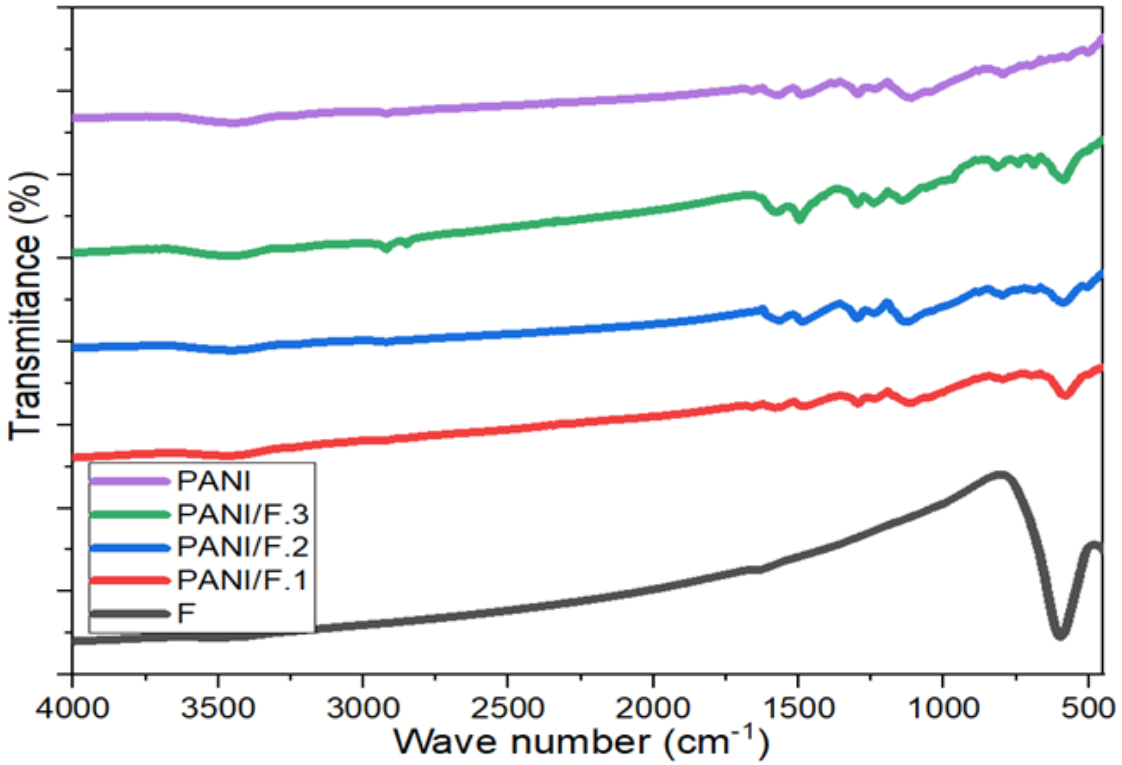

Figure 4: FTIR spectra of $Ni^{3+}_{0.25}Ni^{2+}_{0.375}Zn^{2+}_{0.25}Fe_2O_4$, PANI/$Ni^{3+}_{0.25}Ni^{2+}_{0.375}Zn^{2+}_{0.25}Fe_2O_4$ nanocomposites and pure PANI.

Table 1: TGA measurements of PANI/$Ni^{3+}_{0.25}Ni^{2+}_{0.375}Zn^{2+}_{0.25}Fe_2O_4$ nanocomposites.

Sample	Calculated PANI percentage	Evaluated PANI percentage utilizing TGA
PANI/F.1	50%	53.8%
PANI/F.2	66%	49.5%
PANI/F.3	75%	51.2%

UV–visible spectra

The UV–visible spectrum of the PANI and PANI/F nanocomposites are shown in Fig. 5. For PANI, two characteristic peaks at around 302 nm and 629 nm are observed. The characteristic peak around 302 nm is ascribed to π–π* transition of the benzenoid ring and the characteristic peak around 629 nm is attributed to the benzenoid-to-quinoid excitonic transition [17,24]. It can be seen from Fig. 5 that the characteristic peaks of PANI/F nanocomposites show a clear blue shift of 5 nm, as compared with that of polyaniline. The two characteristic peaks show the presence of PANI on the surface of $Ni^{3+}_{0.25}Ni^{2+}_{0.375}Zn^{2+}_{0.25}Fe_2O_4$. These results may refer the σ–π interaction between $Ni^{3+}_{0.25}Ni^{2+}_{0.375}Zn^{2+}_{0.25}Fe_2O_4$ and polyaniline backbone, which leads the energy of the antibonding orbital decrease, the energy of the π–π* transition of the benzenoid and quinoid ring decreases, so the characteristic peaks of the nanocomposite show a blue shift [24].

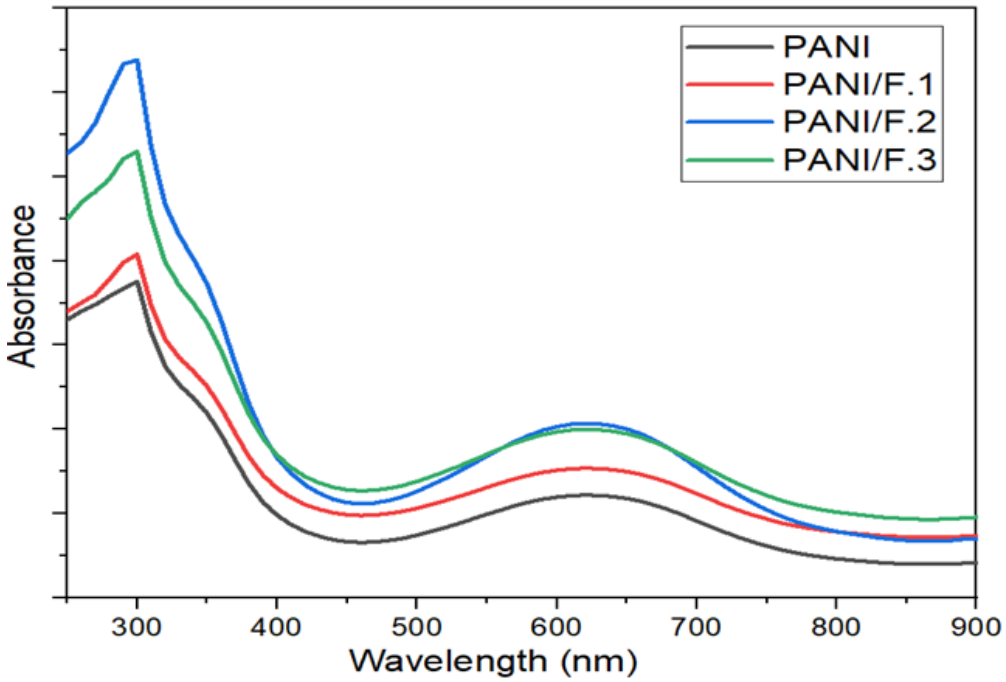

Figure 5: UV spectra of PANI and PANI/$Ni^{3+}_{0.25}Ni^{2+}_{0.375}Zn^{2+}_{0.25}Fe_2O_4$ nanocomposites.

TGA analysis

The TGA curves of the $Ni^{3+}_{0.25}Ni^{2+}_{0.375}Zn^{2+}_{0.25}Fe_2O_4$, PANI/F nanocomposites and polyaniline are shown in Fig. 6. For the $Ni^{3+}_{0.25}Ni^{2+}_{0.375}Zn^{2+}_{0.25}Fe_2O_4$ nanoparticles, no mass loss was noticed over the whole temperature range. PANI loses 4.87% of its weight at the temperature of 110–130 °C which is due to the evaporation of moisture in the PANI. The thermal decomposition of the PANI is shown at the temperature of 230–1000 °C and has a big weight loss of 65.12%. On the other hand, PANI/F nanocomposites lose about of 2.11% of their weight at the temperature of 110–130 °C which is due to the evaporation of moisture in the nanocomposites. The thermal decomposition of the PANI/F nanocomposites is shown at a temperature about of 230–850 °C. The current percentages of PANI in the PANI/F nanocomposites can be evaluated from the TGA curves as shown in Table 1.

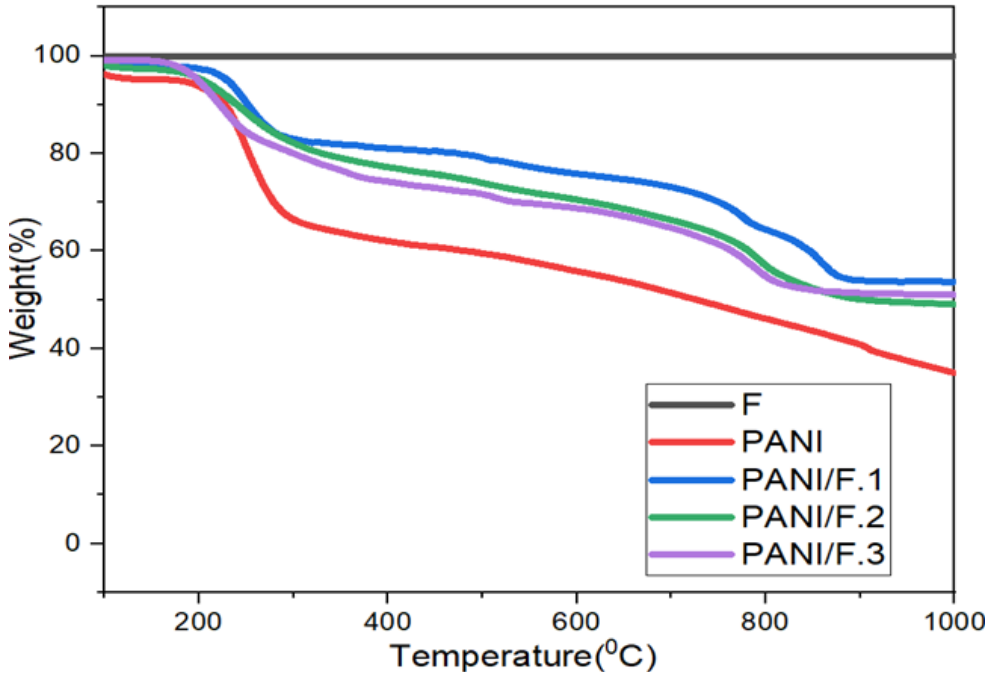

Figure 6: TGA thermograms of $Ni^{3+}_{0.25}Ni^{2+}_{0.375}Zn^{2+}_{0.25}Fe_2O_4$, PANI/$Ni^{3+}_{0.25}Ni^{2+}_{0.375}Zn^{2+}_{0.25}Fe_2O_4$ nanocomposites and pure PANI.

Morphology investigations

The morphology of the $Ni^{3+}_{0.25}Ni^{2+}_{0.375}Zn^{2+}_{0.25}Fe_2O_4$ and PANI is shown in Fig. 7. The agglomerated spherical particles of NiZn ferrite are noticed (Fig. 7 (a)). The average diameters of the spherical-shaped particles are observed to be ranging between 18–93 nm. While a combination of rough surface sheets and short rods connected to each other of PANI are noticed (Fig. 7 (b)), distributed in the range between 60–220 nm. The morphology of various samples of PANI/F nanocomposites is shown in Fig. 8. After coating by polyaniline, a continued overlayer of PANI is created on the $Ni^{3+}_{0.25}Ni^{2+}_{0.375}Zn^{2+}_{0.25}Fe_2O_4$ nanoparticles' surface. The $Ni^{3+}_{0.25}Ni^{2+}_{0.375}Zn^{2+}_{0.25}Fe_2O_4$nanocomposites images exhibit that the $Ni^{3+}_{0.25}Ni^{2+}_{0.375}Zn^{2+}_{0.25}Fe_2O_4$ nanoparticles are coated with PANI to create the composite structure. In addition to that, agglomerated rod-like particles formation is noticed in the PANI/F nanocomposites and this is due to the increased percentage of PANI content in the nanocomposites. One can notice that the percentage of PANI in the PANI/F nanocomposites has a significant role in specifying the definitive morphology of the nanocomposite and this may impact its EMI shielding and MA conduct as will be clarified later.

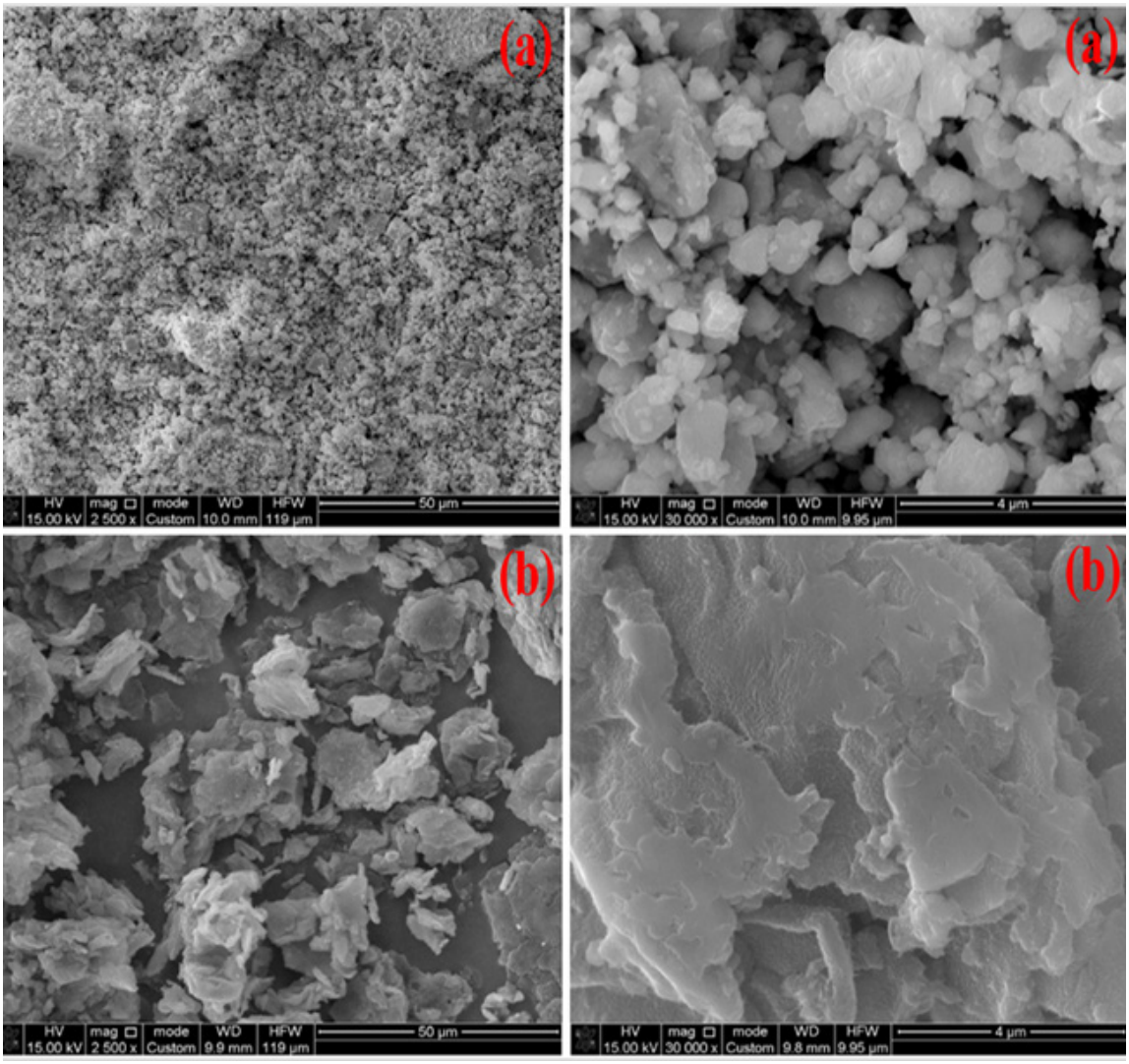

Figure 7: SEM images of (a) $Ni^{3+}_{0.25}Ni^{2+}_{0.375}Zn^{2+}_{0.25}Fe_2O_4$ and (b) PANI on the scale bar of 50 µm and 4 µm.

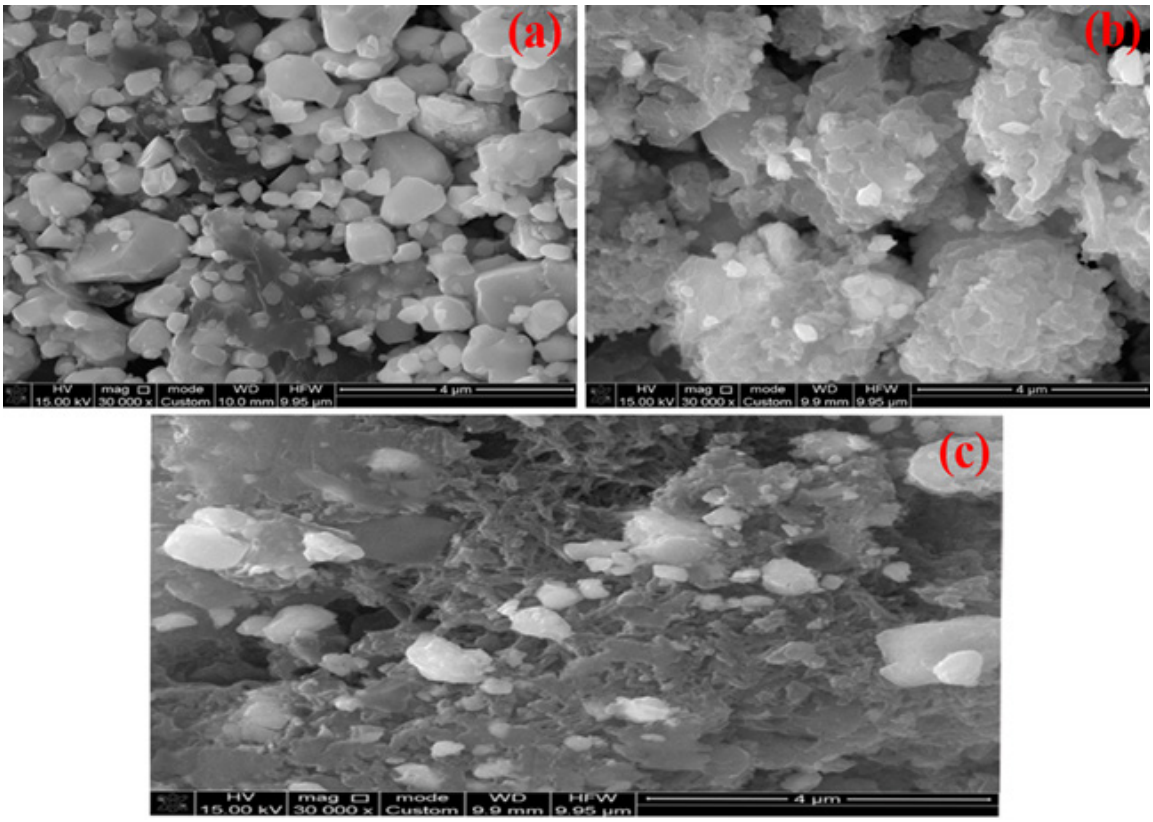

Figure 8: SEM images of (a) PANI/F.1, (b) PANI/F.2 and (c) PANI/F.3.

Energy-dispersive X-ray spectroscopy (EDX) analysis

Energy-dispersive X-ray spectroscopy (EDX) analysis of $Ni^{3+}_{0.25}Ni^{2+}_{0.375}Zn^{2+}_{0.25}Fe_2O_4$, PANI and PANI/F.2 nanocomposite is shown in Fig. 9 and Table 2. The presence of C, O, Cl, S, Fe, Ni, Al and Zn elements in the NiZn ferrite EDX spectrum is noticed. On the other hand, the presence of C, O, S and Cl elements in the PANI EDX spectrum is found. The presence of elemental Cl and S can be attributed to doping agents' hydrochloric acid and sodium dodecyl sulfate. Finally, the presence of C, O, Cl, S, Fe, Zn, Al and Ni elements in the PANI/F.2 nanocomposite EDX spectrum is observed.

Table 2: EDX element composition of $Ni^{3+}_{0.25}Ni^{2+}_{0.375}Zn^{2+}_{0.25}Fe_2O_4$, PANI and PANI/F.2 nanocomposite.

Element	C	Cl	O	S	Al	Fe	Ni	Zn
Ferrite (wt%)	3.28	0.15	19.28	0.03	0.39	53.04	18.02	5.81
PANI (wt%)	84.52	0.45	11.81	3.17	0.05	0	0	0
PANI/F.2 (wt%)	51.76	0.22	19.27	2.42	0.08	17.96	6.32	1.98

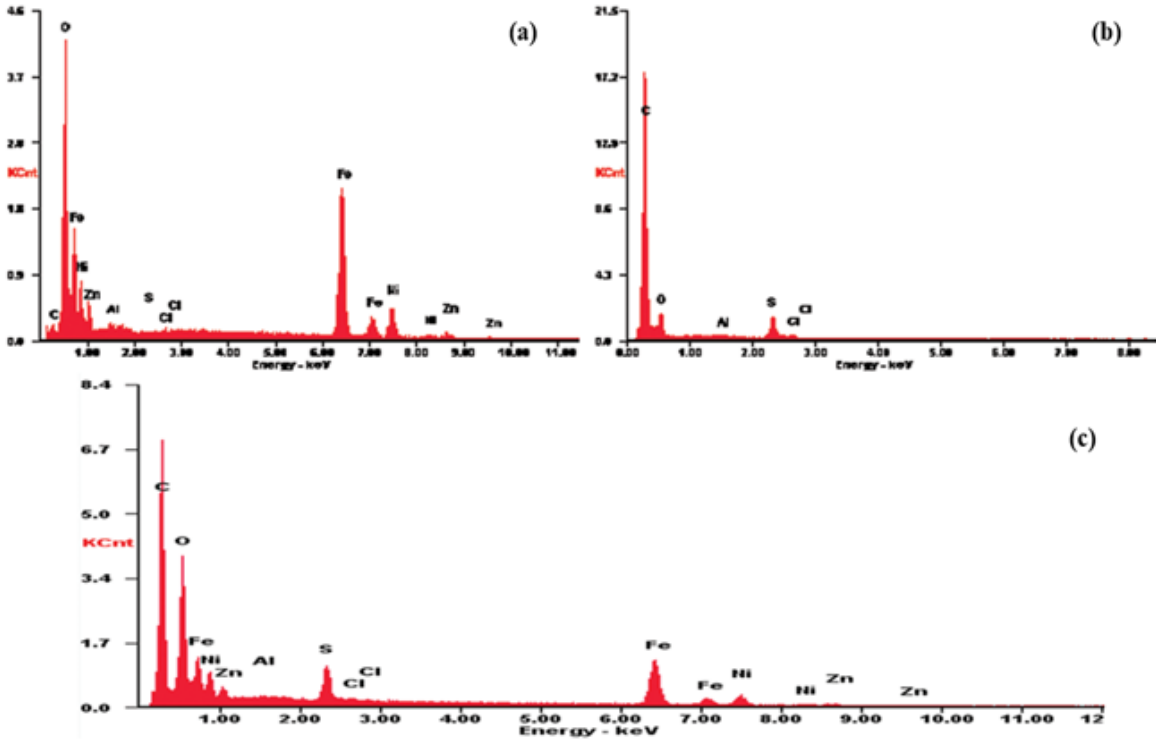

Figure 9: EDX of (a) $Ni^{3+}_{0.25}Ni^{2+}_{0.375}Zn^{2+}_{0.25}Fe_2O_4$, (b) PANI and (c) PANI/F.2 nanocomposite.

EMI shielding and MA properties

There are two general methods that cope with the interference of incident electromagnetic waves: the first one is electromagnetic interference (EMI) shielding and the second one is microwave absorption (MA). For the EMI shielding method (Fig. 10 (a)), the significant point is to attenuate the transmitted power of the EM waves (p_T). On the other hand, for the microwave absorption method (Fig. 10 (b)), though, a metal plate is put to reflect the transmitted power of the EM waves. As a consequence, the transmitted power of the EM waves is negligible in microwave absorption. EMI shielding and MA properties of the prepared samples are estimated with the free-space technique as shown in Fig. 11. EM waves are generated by a microwave generator in the frequency band of 8.8–12 GHz, where a microwave generator is connected by a WR90 waveguide instrument (IEC Standard R100, X Band). The incident EM waves (p_{in}) are measured by the horn antenna connected to an oscilloscope (Fig. 11), then the prepared sample perpendicularly is placed between a microwave generator and the horn antenna to measure the transmitted power of the EM waves (p_T) by an oscilloscope. As a result, SE can be calculated for the EMI shielding by applying the equation (1) [20]:

$$SE\ (dB) = SE_R + SE_A + SE_M = 10\ log\ \frac{p_{in}}{p_T} \quad (1)$$

It is significant to note that the multiple reflection loss (SE_M) can be ignored if the absorption shielding (SE_A) of EMI shielding material is higher than 10 dB and equation (1) then can be rewritten as [20]:

$$SE\ (dB) = SE_R + SE_A = 10\ log\ \frac{p_{in}}{p_T} \quad (2)$$

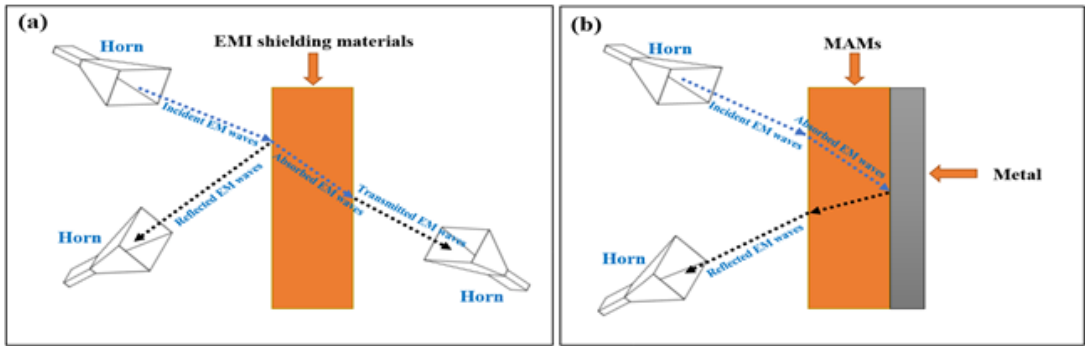

Figure 10: Sketch of the estimate models of (a) electromagnetic interference shielding and (b) microwave absorption.

In addition to that, the reflected power of the EM waves (p_{ref}) is measured when the EM waves are incident on the sample surface at an angle of 45° by an oscilloscope. As a result, the shielding by reflection (SE_R) can be calculated for the EMI shielding by applying the equation (3).

$$SE_R\,(dB) = -10\log(1-R) = -10\log\left(1-\frac{p_{ref}}{p_{in}}\right) \quad (3)$$

Finally, the shielding by absorption (SE_A) is calculated by equation (4) [21,22]:

$$SE_A\,(dB) = -10\log\left(\frac{T}{1-R}\right) = -10\log\left(\frac{p_T}{p_{in}-p_{ref}}\right) \quad (4)$$

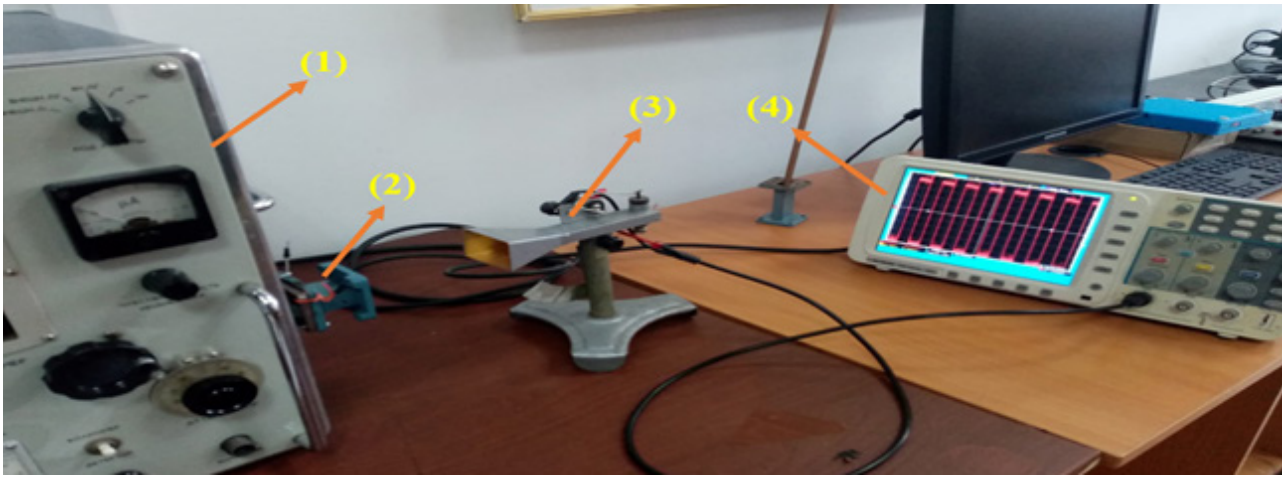

Figure 11: Experimental setup for studying the EMI and MA properties of the prepared samples by the free-space technique. From left to right: (1) microwave generator, (2) waveguide instrument (IEC Standard R100, X Band), (3) horn antenna, and (4) oscilloscope.

For the microwave absorption method, the prepared sample is placed on the metal plate at an angle of 45° to measure the reflected power of the EM waves (p_{ref}) by an oscilloscope. As a result, RL can be calculated by applying the equation (5) [21,22]:

$$Rl\,(dB) = 10log\,\frac{p_{in}}{p_{ref}} \quad (5)$$

Effect of the PANI/$Ni^{3+}_{0.25}Ni^{2+}_{0.375}Zn^{2+}_{0.25}Fe_2O_4$ nanocomposites morphology on the RL and the SE

EMI shielding and MA properties of the $Ni^{3+}_{0.25}Ni^{2+}_{0.375}Zn^{2+}_{0.25}Fe_2O_4$, PANI/F nanocomposites and PANI are studied. The results of this investigation are exhibited in Fig. 12, Fig. 13, and Table 3. Fig. 12 and Fig. 13 illustrate the changing of the RL and SE as a function of the EM wave frequency for various weight ratios of PANI/$Ni^{3+}_{0.25}Ni^{2+}_{0.375}Zn^{2+}_{0.25}Fe_2O_4$ (1:1, 2:1, and 3:1). The absorption of samples with specified thickness at 2.90 mm is molded to measure RL and SE in the frequency band of 8.8–12.0 GHz. As illustrated in Fig. 12 and Fig. 13, for the $Ni^{3+}_{0.25}Ni^{2+}_{0.375}Zn^{2+}_{0.25}Fe_2O_4$ nanoparticles, weak reflection loss and low shielding efficiency are noticed. On the other hand, for the pure PANI, the reflection loss was in the range between 6.2–8.1 dB and the shielding efficiency is in the range between 9.6–12.5 dB. Furthermore, when PANI is incorporated with $Ni^{3+}_{0.25}Ni^{2+}_{0.375}Zn^{2+}_{0.25}Fe_2O_4$ nanoparticles, the reflection loss increases to −18.6 dB at 11.3 GHz for PANI/F.2 nanocomposite and the shielding efficiency increases to 23.18 dB at 11.1 GHz. As for the PANI/F.1 nanocomposite, the reflection loss increases to −15.4 dB at 10.3 GHz and the shielding efficiency increases to 22.1 dB at 11.0 GHz. This indicates that there is a synergistic influence in incorporating $Ni^{3+}_{0.25}Ni^{2+}_{0.375}Zn^{2+}_{0.25}Fe_2O_4$ nanoparticles and PANI. Nevertheless, this increase in RL and SE is not noticed for the PANI/F.3 composite. This refers that the MA and EMI shielding properties being related to the morphology of the nanocomposite. In reality, the mixture of agglomerated particles and rod-like morphology appears to show the best MA and EMI shielding properties. Table 3 shows the low surface density (SD) and the absorption BW_{-10dB} of all the prepared absorbers. the absorption BW_{-10dB} is 1.8 GHz with a surface density of 3.04 for the PANI/F.2 nanocomposite, whereas, the absorption BW-10dB is 1.9 GHz with a surface density of 3.22 for the PANI/F.1 nanocomposite. While no absorption BW-10dB is noticed for PANI, $Ni^{3+}_{0.25}Ni^{2+}_{0.375}Zn^{2+}_{0.25}Fe_2O_4$ and PANI/F.3 nanocomposite. Fig. 14 shows the SER and SEA of PANI/$Ni^{3+}_{0.25}Ni^{2+}_{0.375}Zn^{2+}_{0.25}Fe_2O_4$ nanocomposites with a thickness of 2.90 mm at the frequency of 11.0 GHz.

Table 3: MA behavior of $Ni^{3+}_{0.25}Ni^{2+}_{0.375}Zn^{2+}_{0.25}Fe_2O_4$, PANI/$Ni^{3+}_{0.25}Ni^{2+}_{0.375}Zn^{2+}_{0.25}Fe_2O_4$ nanocomposites and pure PANI at 2.9 mm thickness.

Samples	RL_{min} (dB)	f_m (GHz)	$BW_{-10\ dB}$ (GHz)	SD (kg/m^2)
$Ni^{3+}_{0.25}Ni^{2+}_{0.375}Zn^{2+}_{0.25}Fe_2O_4$	-4.2	-	-	4.53
PANI	-8.1	-	-	2.21
PANI/F.1	-15.4	10.2	1.9	3.22
PANI/F.2	-18.6	11.3	1.8	3.04
PANI/F.3	-8.3	-	-	2.96

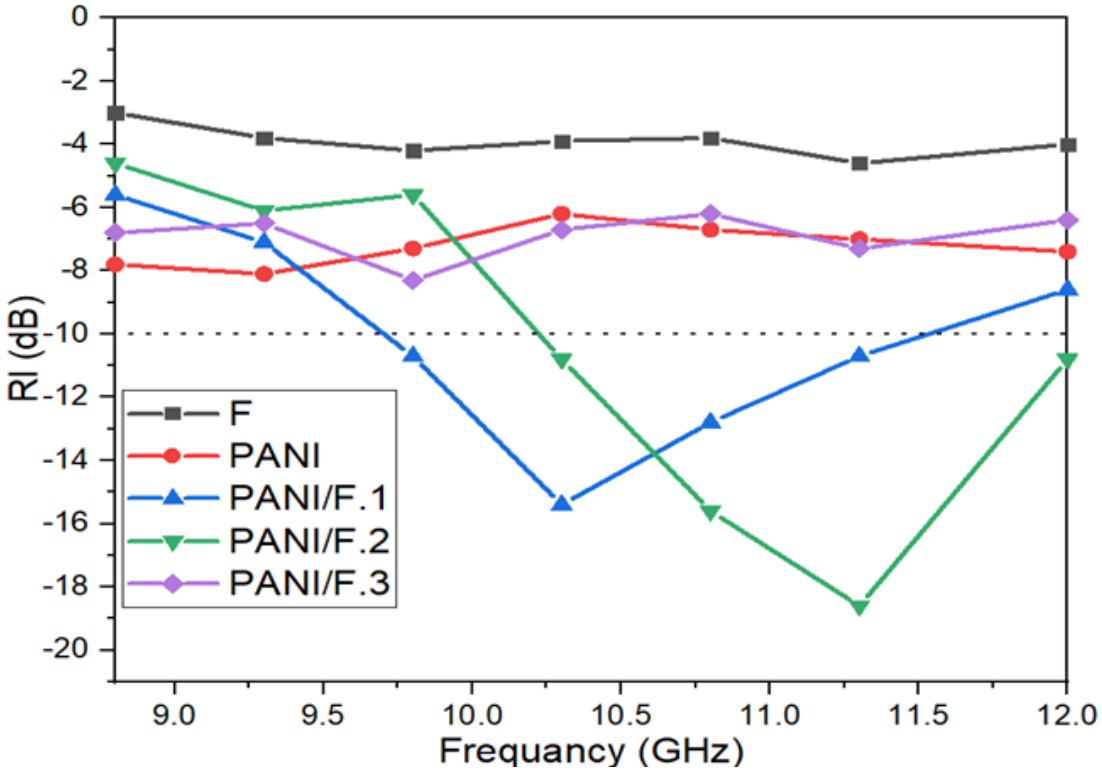

Figure 12: RL curves of $Ni^{3+}_{0.25}Ni^{2+}_{0.375}Zn^{2+}_{0.25}Fe_2O_4$, PANI/$Ni^{3+}_{0.25}Ni^{2+}_{0.375}Zn^{2+}_{0.25}Fe_2O_4$ nanocomposites and pure PANI at 2.9 mm thickness.

Effect of the PANI/ $Ni^{3+}_{0.25}Ni^{2+}_{0.375}Zn^{2+}_{0.25}Fe_2O_4$ nanocomposites thickness on the RL

Fig. 15 illustrates the RL of PANI/F.2 nanocomposite with different thicknesses at the weight percentage of the absorber within a paraffin matrix (25% w/w). Fig. 15 illustrates that the RL attenuation peaks of samples moved to lower frequencies with increasing sample thickness. This phenomenon may be defined by the quarter-wavelength (λ/4) cancellation model, as shown in equation (6) [28–30]:

$$t_m = \frac{c}{4f_m\sqrt{|\mu_r||\varepsilon_r|}} \quad (6)$$

Where |εr| and |μr| are the modulus of the measured complex relative permittivity (ε_r) and permeability (μ_r) at matching frequency (f_m), respectively. c is the velocity of light.

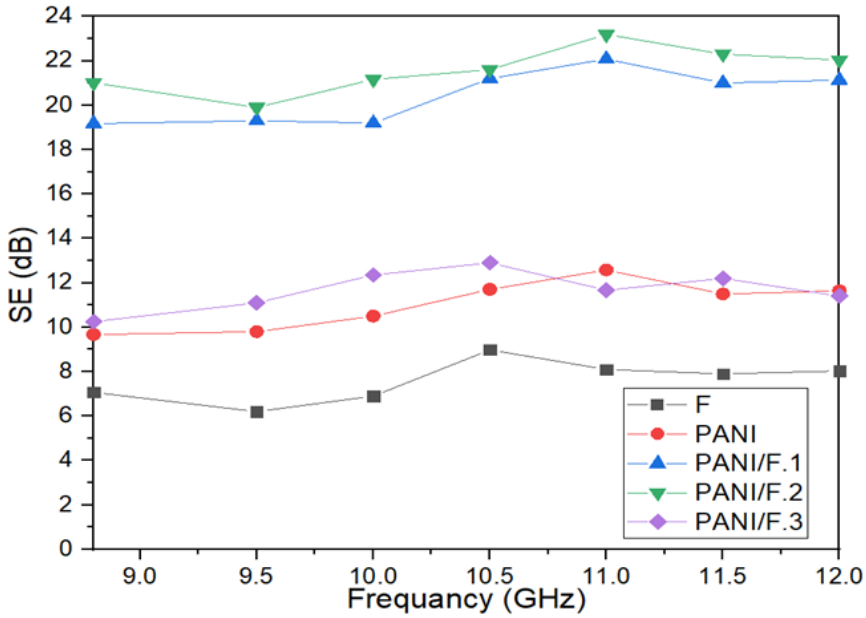

Figure 13: SE curves of $Ni^{3+}_{0.25}Ni^{2+}_{0.375}Zn^{2+}_{0.25}Fe_2O_4$, PANI/$Ni^{3+}_{0.25}Ni^{2+}_{0.375}Zn^{2+}_{0.25}Fe_2O_4$ nanocomposites and pure PANI at 2.9 mm thickness.

It can be noticed from equation (7) that the fm is inversely proportionate to the thickness of an absorber. One can conclude that the optimal matching and absorption can be accomplished by modifying the fm and the tm of an absorber (Table 4).

Table 4: MA behavior of PANI/F.2 nanocomposite at various thicknesses.

PANI/F.2	t (mm)	RL_{min} (dB)	f_m (GHz)	BW_{-10dB} (GHz)	SD (kg/m^2)
	2.90	-18.6	11.3	1.8	3.04
	3.12	-19.8	10.8	2.2	3.07
	3.46	-15.7	10.2	2.7	3.09
	3.62	-16.9	9.3	1.7	3.12

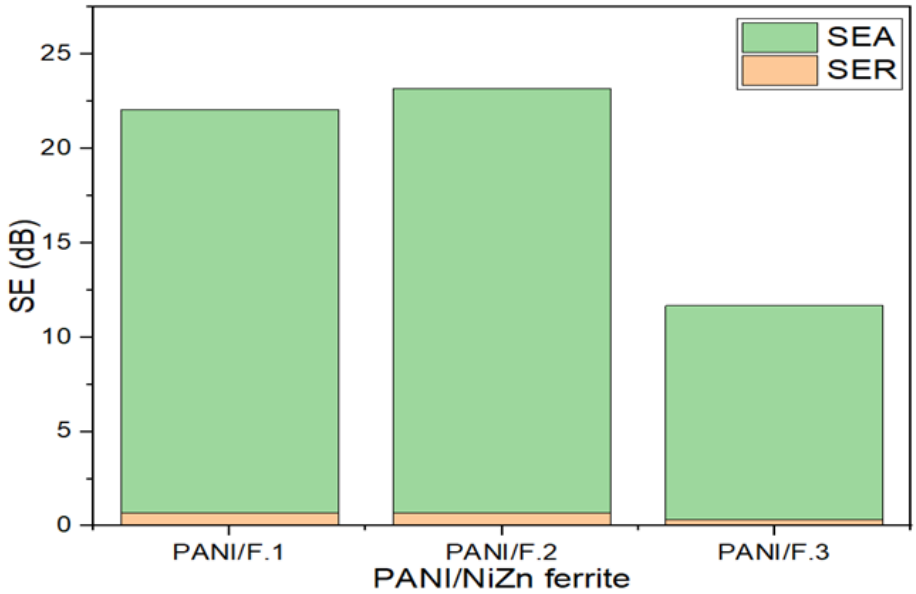

Figure 14: Bar plot for individual components of SER and SEA of PANI/$Ni^{3+}_{0.25}Ni^{2+}_{0.375}Zn^{2+}_{0.25}Fe_2O_4$ nanocomposites with a thickness of 2.90 mm at the frequency of 11.0 GHz.

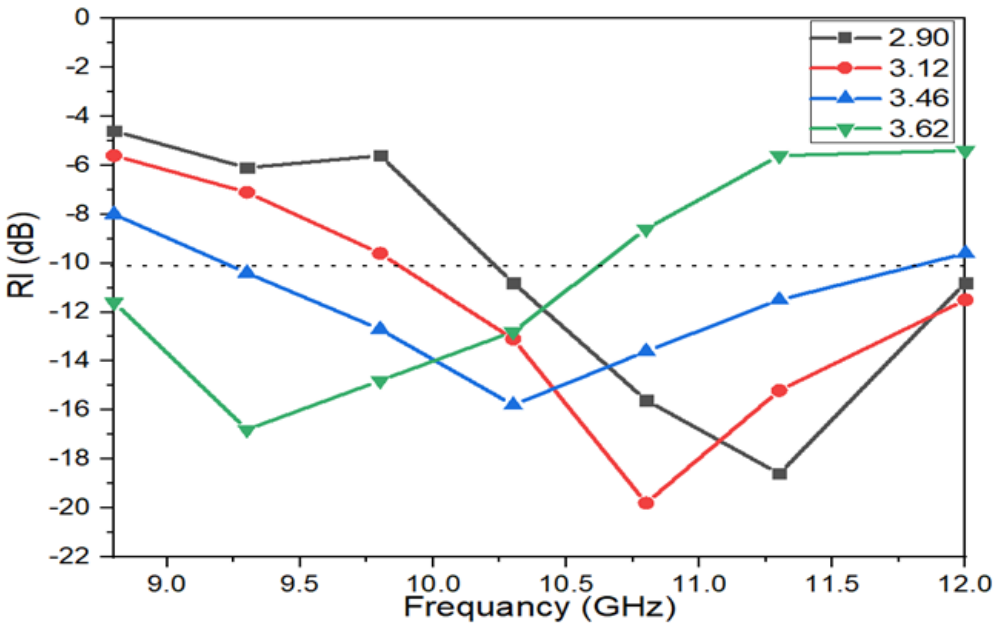

Figure 15: RL curves of PANI/F.2 nanocomposite at various thicknesses.

Conclusion

In the current research, PANI/$Ni^{3+}_{0.25}Ni^{2+}_{0.375}Zn^{2+}_{0.25}Fe_2O_4$ microwave absorbers were successfully synthesized and characterized by XRD, FTIR spectroscopy, UV–vis spectroscopy, TGA analysis and SEM analysis. The functional characterization was accomplished by measuring the EMI shielding and MA properties. $Ni^{3+}_{0.25}Ni^{2+}_{0.375}Zn^{2+}_{0.25}Fe_2O_4$ was used to enhance the mechanism of magnetic loss, while PANI was introduced to enhance the mechanism of dielectric loss. As a result, one can notice the impact of combining $Ni^{3+}_{0.25}Ni^{2+}_{0.375}Zn^{2+}_{0.25}Fe_2O_4$ and PANI on the EMI and MA properties of the absorber. This combination drives to an effective and low thickness absorber with minimal reflection loss. The low loading ratio of $Ni^{3+}_{0.25}Ni^{2+}_{0.375}Zn^{2+}_{0.25}Fe_2O_4$ nanoparticles coated with polyaniline within paraffin wax matrix (25% w/w) permits the synthesis of a lightweight microwave absorption material. The results refer that MA and EMI shielding properties being related to the morphology of the nanocomposite and the thickness of the absorption material. The RLmin of -19.8 dB at the fm of 10.8 GHz and the absorption BW-10dB of 2.2 GHz for 3.12 mm thickness with a surface density of 3.07 kg/m^2 is noticed for the PANI/F.2 nanocomposite sample. The maximum SE of 23.18 dB at 11.1 GHz for 2.90 mm thickness is observed for the PANI/F.2 nanocomposite.

Acknowledgments

The authors express their gratitude to Al-Farabi Kazakh National University, the center of complex processing of mineral raw materials, and the center of physical-chemical methods of research and analyses for providing the materials and equipment to conduct this research project.

References

1. Aldashevich, Z., Saule, M. I. R. Z. A. L. I. E. V. A., & Telmanovna, B. (2022). Microwave absorption behavior of low loading ratio of $Ni^{3+}_{0.25}Ni^{2+}_{0.375}Zn^{2+}_{0.25}Fe_2O_4$ nanoparticles coated with polyaniline within paraffin wax matrix.
2. Liang, C., Qiu, H., Song, P., Shi, X., Kong, J., & Gu, J. (2020). Ultra-light MXene aerogel/wood-derived porous carbon composites with wall-like “mortar/brick” structures for electromagnetic interference shielding. Science Bulletin, 65(8), 616-622.
3. Chen, X., Shi, T., Zhong, K., Wu, G., & Lu, Y. (2020). Capacitive behavior of MoS2 decorated with FeS2@ carbon nanospheres. Chemical Engineering Journal, 379, 122240.
4. Chen, S., Meng, G., Kong, B., Xiao, B., Wang, Z., Jing, Z., ... & Cheng, Y. (2020). Asymmetric alicyclic amine-polyether amine molecular chain structure for improved energy storage density of high-temperature crosslinked polymer capacitor. Chemical Engineering Journal, 387, 123662.
5. Cheng, C., Chen, Z., Huang, Z., Zhang, C., Tusiime, R., Zhou, J., ... & Zhang, H. (2020). Simultaneously improving mode I and mode II fracture toughness of the carbon fiber/epoxy composite laminates via interleaved with uniformly aligned PES fiber webs. Composites Part A: Applied Science and Manufacturing, 129, 105696.
6. Xu, H., Yin, X., Li, X., Li, M., Liang, S., Zhang, L., & Cheng, L. (2019). Lightweight Ti2CT x MXene/poly (vinyl alcohol) composite foams for electromagnetic wave shielding with absorption-dominated feature. ACS applied materials & interfaces, 11(10), 10198-10207.
7. Houbi, A., Aldashevich, Z. A., Atassi, Y., Telmanovna, Z. B., Saule, M., & Kubanych, K. (2021). Microwave absorbing properties of ferrites and their composites: A review. Journal of Magnetism and Magnetic Materials, 529, 167839.
8. Harris, V. G. (2011). Modern microwave ferrites. IEEE Transactions on Magnetics, 48(3), 1075-1104.

9. Cui, G., Lu, Y., Zhou, W., Lv, X., Hu, J., Zhang, G., & Gu, G. (2019). Excellent microwave absorption properties derived from the synthesis of hollow Fe3O4@ reduced graphite oxide (RGO) nanocomposites. Nanomaterials, 9(2), 141.
10. Luo, J., Zuo, Y., Shen, P., Yan, Z., & Zhang, K. (2017). Excellent microwave absorption properties by tuned electromagnetic parameters in polyaniline-coated Ba 0.9 La 0.1 Fe 11.9 Ni 0.1 O 19/reduced graphene oxide nanocomposites. RSC advances, 7(58), 36433-36443.
11. Ali, N. N., Atassi, Y., Salloum, A., Malki, A., Jafarian, M., & Almarjeh, R. K. B. (2019). Lightweight broadband microwave absorbers of core–shell (polypyrrole/NiZn ferrite) nanocomposites in the X-band: insights on interfacial polarization. Journal of Materials Science: Materials in Electronics, 30(7), 6876-6887.
12. Ting, T. H., Yu, R. P., & Jau, Y. N. (2011). Synthesis and microwave absorption characteristics of polyaniline/NiZn ferrite composites in 2–40 GHz. Materials Chemistry and Physics, 126(1-2), 364-368.
13. Ali, N. N., Al-Marjeh, R. A. Q. B., Atassi, Y., Salloum, A., Malki, A., & Jafarian, M. (2018). Design of lightweight broadband microwave absorbers in the X-band based on (polyaniline/MnNiZn ferrite) nanocomposites. Journal of Magnetism and Magnetic Materials, 453, 53-61.
14. Wang, C. P., Li, C. H., Bi, H., Li, J. C., Zhang, H., Xie, A. J., & Shen, Y. H. (2014). Novel one-dimensional polyaniline/Ni0. 5Zn0. 5Fe_2O_4 hybrid nanostructure: synthesis, magnetic, and electromagnetic wave absorption properties. Journal of nanoparticle research, 16(3), 1-11.
15. Wang, M., Ji, G., Zhang, B., Tang, D., Yang, Y., & Du, Y. (2015). Controlled synthesis and microwave absorption properties of Ni0. 6Zn0. 4Fe_2O_4/PANI composite via an in-situ polymerization process. Journal of Magnetism and Magnetic Materials, 377, 52-58.
16. El Nahrawy, A. M., Salah El-Deen, H., Soliman, A. A., & Mosa, W. M. (2019). Crystallographic and magnetic properties of Al3+ co-doped NiZnFe2O4 nano-particles prepared by sol-gel process. Egyptian Journal of Chemistry, 62(3), 525-532.
17. Ezzati, S. N., Rabbani, M., Leblanc, R. M., Asadi, E., Ezzati, S. M. H., Rahimi, R., & Azodi-Deilami, S. (2015). Conducting, magnetic polyaniline/Ba0. 25Sr0. 75 Fe11 (Ni0. 5Mn0. 5) O19 nanocomposite: fabrication, characterization and application. Journal of Alloys and Compounds, 646, 1157-1164.
18. Meng, X., Zhu, Y., Xu, S., & Liu, T. (2016). Facile synthesis of shell–core polyaniline/SrFe 12 O 19 composites and magnetic properties. RSC advances, 6(6), 4946-4949.
19. Ali, N. N., Atassi, Y., Salloum, A., Charba, A., Malki, A., & Jafarian, M. (2018). Comparative study of microwave absorption characteristics of (Polyaniline/NiZn ferrite) nanocomposites with different ferrite percentages. Materials Chemistry and Physics, 211, 79-87.
20. Elsayed, A. H., Eldin, M. M., Elsyed, A. M., Elazm, A. A., Younes, E. M., & Motaweh, H. A. (2011). Synthesis and properties of polyaniline/ferrites nanocomposites. Int. J. Electrochem. Sci, 6(1), 206-221.
21. Kondawar SB, Nandapure AI. (2014). Magnetic and electrical properties of zinc-substituted nickel ferrite reinforced conducting polyaniline nanocomposites. J Chinese Adv Mater Soc, 2, 186–98.
22. Gairola, S. P., Verma, V., Kumar, L., Dar, M. A., Annapoorni, S., & Kotnala, R. K. (2010). Enhanced microwave absorption properties in polyaniline and nano-ferrite composite in X-band. Synthetic Metals, 160(21-22), 2315-2318.
23. Li, G., Yan, S., Zhou, E., & Chen, Y. (2006). Preparation of magnetic and conductive NiZn ferrite-polyaniline nanocomposites with core-shell structure. Colloids and Surfaces A: Physicochemical and Engineering Aspects, 276(1-3), 40-44.
24. Li, L., Jiang, J., & Xu, F. (2007). Synthesis and ferrimagnetic properties of novel Sm-substituted LiNi ferrite–polyaniline nanocomposite. Materials Letters, 61(4-5), 1091-1096.
25. Li, L., Jiang, J., & Xu, F. (2007). Synthesis and ferrimagnetic properties of novel Sm-substituted LiNi ferrite–polyaniline nanocomposite. Materials Letters, 61(4-5), 1091-1096.
26. Bayat, M., Yang, H., Ko, F. K., Michelson, D., & Mei, A. (2014). Electromagnetic interference shielding effectiveness of hybrid multifunctional Fe_3O_4/carbon nanofiber composite. Polymer, 55(3), 936-943.
27. Hong, Y. K., Lee, C. Y., Jeong, C. K., Lee, D. E., Kim, K., & Joo, J. (2003). Method and apparatus to measure electromagnetic interference shielding efficiency and its shielding characteristics in broadband frequency ranges. Review of scientific instruments, 74(2), 1098-1102.
28. Wang, S., Jiao, Q., Shi, Q., Zhu, H., Feng, T., Lu, Q., ... & Zhao, Y. (2020). Synthesis of porous nitrogen-doped graphene decorated by γ-Fe_2O_3 nanorings for enhancing microwave absorbing performance. Ceramics International, 46(1), 1002-1010.
29. Shu, R., Zhang, J., Guo, C., Wu, Y., Wan, Z., Shi, J., ... & Zheng, M. (2020). Facile synthesis of nitrogen-doped reduced graphene oxide/nickel-zinc ferrite composites as high-performance microwave absorbers in the X-band. Chemical Engineering Journal, 384, 123266.
30. Jaiswal, R., Agarwal, K., Kumar, R., Kumar, R., Mukhopadhyay, K., & Prasad, N. E. (2020). EMI and microwave absorbing efficiency of polyaniline-functionalized reduced graphene oxide/γ-Fe_2O_3 /epoxy nanocomposite. Soft Matter, 16(28), 6643-6653.